

The zirconium–platinum phase diagram

J.K. Stalick^{a,*}, R.M. Waterstrat^b

^a NIST Center for Neutron Research, National Institute of Standards and Technology, Gaithersburg, MD 20899, USA

^b Metallurgy Division, National Institute of Standards and Technology, Gaithersburg, MD 20899, USA

Received 4 April 2006; received in revised form 21 April 2006; accepted 24 April 2006

Available online 23 June 2006

Abstract

Phase relationships were studied in Pt-rich, near-equiatomic Zr–Pt alloys. The composition range of the previously unreported rhombohedral compound Zr_3Pt_4 , isomorphous with Zr_3Pd_4 above room temperature, extends to the Zr-rich composition Zr_9Pt_{11} by the formation of lattice vacancies on certain Pt sites. A metastable tetragonal Zr_9Pt_{11} compound is formed, however, when vacancy formation is inhibited. The rhombohedral structure undergoes a displacement transformation on cooling between 90 and 140 °C to a low-temperature structure that is presumably triclinic. The orthorhombic compound ZrPt is stable from room temperature to 1590 °C where it transforms to a cubic B2-type structure. Structural data are given for the compounds ZrPt, Zr_9Pt_{11} , Zr_3Pt_4 and Zr_7Pt_{10} , and a complete Zr–Pt phase diagram is presented.

© 2006 Elsevier B.V. All rights reserved.

Keywords: Intermetallics; Crystal structure and symmetry; Neutron diffraction; Phase diagram; Pt alloys; Zr alloys

1. Introduction

It has been noted that binary alloys that combine an early and a late transition element have large negative enthalpies of formation [1,2]. Many of these alloys form B2 compounds and undergo martensitic transformations over a wide range of temperatures. We have typically observed that those materials with high martensitic transformation temperatures are brittle and those with low transformation temperatures are softer and more ductile. The compound ZrPt, therefore, is expected to be brittle since the transformation temperature is high (see Section 3.1).

The equiatomic region of the Zr–Pt phase diagram has never been properly investigated. Kendall et al. [3] have published a phase diagram for the Zr-rich alloys up to 50 atom fraction Pt. Fairbank et al. [4] have reported a phase diagram for Pt-rich alloys up to 25 atom fraction Zr. Raman and Schubert [5] reported compounds at the compositions ZrPt, “ZrPt₊” (Pt-rich ZrPt), Zr_4Pt_5 and “Zr₂Pt₃₋” (Pt-poor Zr_2Pt_3) but gave little additional information about them. The compound ZrPt was later identified as a CrB-type structure [6], the compound Zr_4Pt_5 was identified as a tetragonal Zr_9Pt_{11} -type structure [7] and

“Zr₂Pt₃₋” was identified as an orthorhombic Zr_7Ni_{10} -type structure [7].

The purpose of the present study was to clarify the phase relationships in the Pt-rich near-equiatomic Zr–Pt alloys and to determine their crystal structures.

2. Experimental procedures

All samples were prepared by arc-melting in a 50% argon–helium atmosphere. Melting losses were always less than 1%. The starting materials were Pt wire of 99.9% purity and iodide process (crystal bar) Zr of 99.95% purity containing less than 0.1% Hf. In most cases the sample was arc-cast in a water-cooled copper mold to obtain a cylindrical rod of 0.635 cm (1/4 in.) diameter and 5–7.5 cm in length. These samples were annealed in a high vacuum furnace having heating elements of pure Ta. Samples were cooled by turning off the furnace power, resulting in relatively rapid cooling to near room temperature in approximately 10 min. Temperatures were measured with an accuracy of ± 10 °C by calibrating furnace current against the observed melting points of secondary standards such as Au, Ni, Pt and Rh. Solidus temperatures were determined by visual observations of incipient melting on samples supported by ceramic crucibles or suspended with thin W wire. Several alloys were initially annealed at 1600 °C for 1 h. Samples for metallographic examination were etched with a 50% aqueous solution of HF in an electrolytic apparatus using 5–10 V ac power.

X-ray diffraction patterns were taken at room temperature using Cu K α radiation. Powder samples for X-ray diffraction studies were prepared by grinding or filing. Internal strain was relieved by annealing the powder in Ta foil containers.

Neutron diffraction data were collected using the BT-1 32-detector powder diffractometer at the NIST Center for Neutron Research. Data were collected using either a Cu(3 1 1) monochromator with a take-off angle of 90° and a neutron

* Corresponding author. Tel.: +1 301 9756223; fax: +1 301 9219847.
E-mail address: judith.stalick@nist.gov (J.K. Stalick).

wavelength of 1.5401(1) Å or 1.5394(1) Å, or with a Ge(3 1 1) monochromator with a 75° take-off angle and a neutron wavelength of 2.0775(1) Å. The in-pile collimation used was 15' of arc. Data were collected over the range 3–168° 2θ using the Cu(3 1 1) monochromator or 1.8–166.8° 2θ using the Ge(3 1 1) monochromator, with a step size of 0.05°. High-temperature data in the range 300–1620 °C were obtained using a vacuum furnace with a Nb heating element, with the sample suspended by W–Re wire. At intermediate (up to 327 °C) and low temperatures the samples were sealed under He atmosphere in vanadium sample containers, and temperature control was obtained using a closed-cycle refrigerator. In all cases samples were held at temperature until no further changes in the diffraction pattern were observed, as determined by repeat diffraction scans prior to data collection. This time was typically 3–6 h.

The crystallographic structural parameters were refined using the Rietveld technique as implemented in the GSAS suite of programs [8]. In most cases it was possible to quantify all phases present using multi-phase refinement of the crystal structures of the constituent phases. It was necessary at times to correct for preferred orientation effects after the samples had been held at the highest temperatures.

Energy dispersive spectroscopy (EDS) was used to determine that a composition range exists for the compound ZrPt₃. This phase is not discussed further in this paper.

3. Results

Preliminary studies had indicated that we could expect to find compounds at the compositions ZrPt, Zr₉Pt₁₁, Zr₃Pt₄ and Zr₇Pt₁₀. Samples were therefore prepared at these four compositions. In addition, we prepared a sample at the composition

Zr₄₇Pt₅₃ to aid in the interpretation of the phase equilibria in the equiatomic region. All five samples were examined using high-temperature neutron diffraction, X-ray diffraction and optical microscopy. The results were as follows.

3.1. ZrPt

The cast sample was initially annealed at 1200 °C for 1.5 h, primarily to relieve strains and stabilize the structure which already appeared to be homogeneous. A room-temperature neutron diffraction pattern was obtained, and the crystal structure was refined as orthorhombic CrB-type, space group *Cmcm*. Crystallographic data obtained from this and subsequent neutron Rietveld refinements are given in Table 1. A few small peaks that could not be ascribed to any known impurity phase remained unindexed; however, the fit of calculated and observed patterns was quite good (Fig. 1). High-temperature neutron data sets at 600 and 1405 °C did not exhibit these additional reflections. The orthorhombic structure appeared to be stable up to 1575 °C, but at 1590 ± 10 °C was replaced by a cubic B2 structure with $a = 3.385(1)$ Å. The orthorhombic structure reappeared on cooling, along with the previously mentioned unindexed reflections, and the sample microstructure appeared typically martensitic.

Since it has recently been suggested that ZrPt might undergo a phase transformation from lower symmetry (perhaps mono-

Table 1
Crystallographic data for Zr–Pt compounds

Sample	Space group	Structure type	a (Å) α	b (Å) β	c (Å) γ	V (Å ³)	Z	T (°C)
ZrPt	<i>Cmcm</i>	CrB ^a	3.4082(2)	10.300(1)	4.2806(3)	150.3	4	20
	<i>Cmcm</i>	CrB	3.4261(2)	10.332(1)	4.3110(3)	152.6	4	600
			3.4542(2)	10.372(1)	4.3578(3)	156.1	4	1405
	<i>Pm3m</i>	B2	3.385(1)			38.8	1	1590
Zr ₄₇ Pt ₅₃	<i>Pm3m</i>	B2	3.379(1)			38.6		1550
Zr ₉ Pt ₁₁	<i>P4/m</i>	Type ^a	10.356(1)		6.913(1)	741.4	2	20 ^b
			10.449(1)		6.972(1)	761.4	2	1000
Zr ₉ Pt ₁₁ (annealed)	<i>P1</i>	Zr ₃ Pt ₄	7.520(1)	7.342(1)	7.397(1)	246.9	2/3	20
			111.4(1)	114.7(1)	116.1(1)			
			7.508(1)	7.358(1)	7.420(1)	247.6	2/3	140 ^b
	<i>R3</i>	Pu ₃ Pd ₄	111.9(1)	114.7(1)	115.6(1)			
			12.446(1)		5.536(1)	747.9	2	140 ^b
			12.473(1)		5.551(1)	747.9	2	300
			12.572(1)		5.597(1)	766.1	2	1200
Zr ₃ Pt ₄	<i>P1</i>	Type	7.513(1)	7.388(1)	7.485(1)	249.6	2	27
			111.7(1)	115.1(1)	115.6(1)			
			7.517(1)	7.404(1)	7.484(1)	250.1	2	70 ^b
			112.0(1)	114.9(1)	115.6(1)			
	<i>R3</i>	Pu ₃ Pd ₄	12.522(1)		5.528(1)	750.6	6	70 ^b
			12.558(1)		5.545(1)	757.4	6	300
			12.587(1)		5.559(1)	762.7	6	600
			12.651(1)		5.601(1)	776.3	6	1200
			12.683(1)		5.632(1)	784.5	6	1500
Zr ₇ Pt ₁₀	<i>Cmca</i>	Zr ₇ Ni ₁₀ ^a	13.087(2)	9.613(1)	9.612(1)	1209.2	4	20

Standard uncertainties are given in parentheses. Angles are given only when not fixed by lattice symmetry. Where data have been obtained over a broad temperature range, only data at selected temperatures are given.

^a Structure type is not certain (see text).

^b Multi-phase sample.

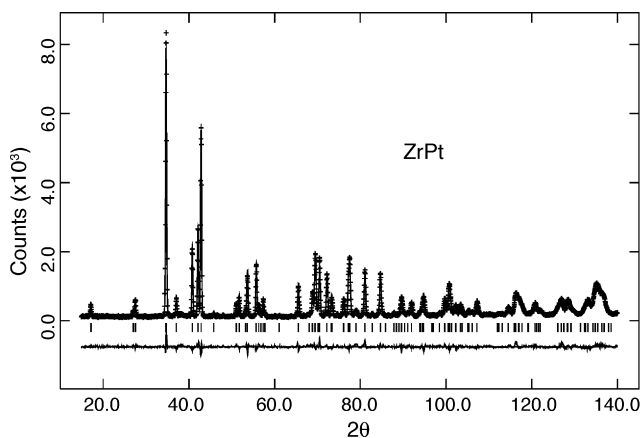


Fig. 1. Observed (+), calculated (solid line), and difference (bottom line) intensities for a portion of the neutron diffraction pattern of ZrPt at room temperature, $\lambda = 1.5398 \text{ \AA}$. Vertical bars mark calculated reflection positions. Pt and Zr atoms are in positions $4c (0, y, 1/4)$ with refined parameters $y = 0.0904(1)$ for Pt and $y = 0.3582(1)$ for Zr.

clinic) to orthorhombic near $573 \text{ K} (300 \text{ }^\circ\text{C})$ [9], several neutron diffraction patterns were taken above and below this temperature. The data were obtained on the cast sample, which had formed large crystallites at high temperature during the previous neutron diffraction experiment, and on the same sample after ball-milling. We were unable to obtain strong evidence of a phase transformation in the range $200\text{--}500 \text{ }^\circ\text{C}$. However, the small unindexed reflections clearly remain below $200 \text{ }^\circ\text{C}$ and are not observed above $500 \text{ }^\circ\text{C}$. These peaks could not be indexed based upon a monoclinic lattice similar to that found for ZrPd [10], and would require a lattice of four times the primitive unit-cell volume of the CrB-type structure in order to be indexed. However, we cannot exclude the possibility that these peaks may result from an unknown impurity phase. Single-crystal work is needed to confirm the hypothesis of lower symmetry and larger unit cell.

3.2. $\text{Zr}_{47}\text{Pt}_{53}$

This sample was examined in the as-cast condition with the aim of observing its behavior at high temperature. The as-cast structure consisted of martensitic platelets of the orthorhombic CrB-type phase of ZrPt interspersed with the phase Zr_3Pt_4 (Fig. 2). The Zr_3Pt_4 phase will be discussed in a later section. Neutron Rietveld refinement indicated approximately equal amounts of these two phases, along with about 12% tetragonal $\text{Zr}_9\text{Pt}_{11}$ and other unidentified phases. There were minor changes in this mixed structure as it was heated, with the Zr_3Pt_4 phase showing some apparent structural changes. The CrB-type phase persisted until $1550 \pm 10 \text{ }^\circ\text{C}$ where it was replaced by a modified cubic B2 structure with $a = 3.379(1) \text{ \AA}$. The pattern (Fig. 3) now exhibited sharp satellite peaks. It should be noted that the relative intensities of the main diffraction peaks and satellite peaks may be altered by the formation of large single-crystal grains at this high temperature. The origin of the satellite peaks is not well understood but is believed to be associated with structural instability produced by the presence of anti-site

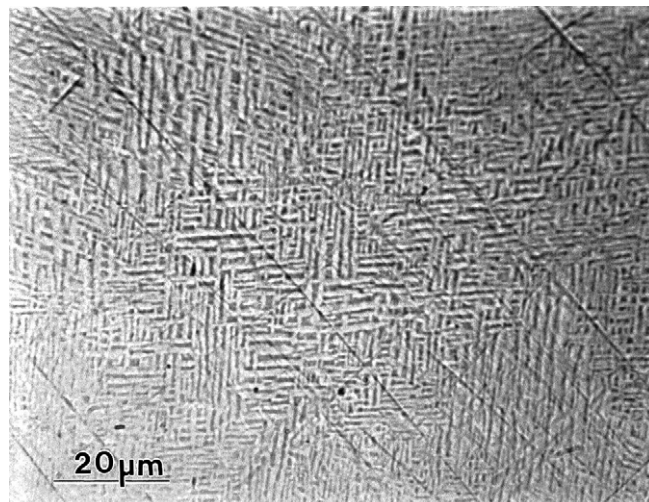


Fig. 2. Photomicrograph of as-cast $\text{Zr}_{47}\text{Pt}_{53}$. The Widmanstatten structure, derived from the prior B2 phase, consists of martensitic ZrPt interspersed with triclinic/rhombohedral Zr_3Pt_4 .

Pt atoms, which replace some Zr atoms of the ideal B2 structure. The possibility that these peaks are due to a lattice displacement wave cannot be ruled out; however, we were only able to examine this structure over a small temperature range ($1560\text{--}1620 \text{ }^\circ\text{C}$) which was insufficient to detect any changes in the positions of the satellite peaks with temperature. The additional peaks could not be ascribed to any known impurity phase.

A portion of this sample was later annealed at $1200 \text{ }^\circ\text{C}$ for 7 days and re-examined at room temperature. The microstructure (Fig. 4) was very similar to that shown in Fig. 2 but now the interplatelet material had a tetragonal $\text{Zr}_9\text{Pt}_{11}$ structure (see below) along with the orthorhombic CrB-type ZrPt. This was confirmed by a neutron diffraction experiment in which the original sample was again studied using the high-temperature furnace to $1200 \text{ }^\circ\text{C}$ and cooled in the furnace to room temperature. Subsequent Rietveld refinement using neutron diffraction data taken at room temperature showed that the sample consisted of 54 wt.% orthorhombic ZrPt and 46 wt.% tetragonal $\text{Zr}_9\text{Pt}_{11}$, consistent with the metallographic results.

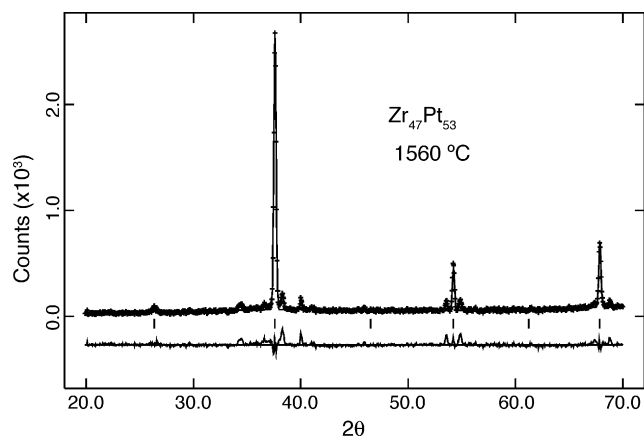


Fig. 3. Neutron diffraction pattern ($\lambda = 1.5403 \text{ \AA}$) for $\text{Zr}_{47}\text{Pt}_{53}$ at $1560 \text{ }^\circ\text{C}$ showing additional satellite reflections. Intensities were calculated for a B2-type structure with Zr at $(0, 0, 0)$ and Pt at $(1/2, 1/2, 1/2)$.

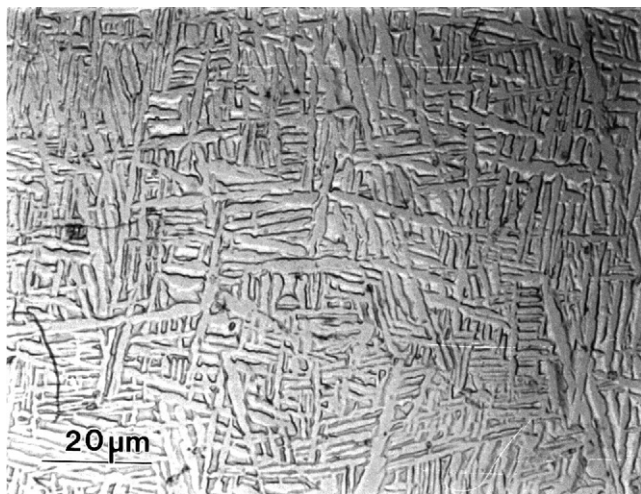


Fig. 4. Photomicrograph of $Zr_{47}Pt_{53}$ annealed at $1200\text{ }^{\circ}\text{C}$ for 7 days, showing martensitic ZrPt interspersed with tetragonal Zr_9Pt_{11} .

3.3. Zr_9Pt_{11}

Panda and Bahn [7] reported that they had prepared a sample which produced only diffraction lines of the tetragonal Zr_9Pt_{11} structure (space group $I4/m$) by annealing a cast sample at $1200\text{ }^{\circ}\text{C}$ for 1 h. We annealed an arc-cast sample at $1200\text{ }^{\circ}\text{C}$ for 1.5 h and obtained about 85 wt.% of the tetragonal phase with the remainder being a mixture of triclinic Zr_3Pt_4 (see Section 3.4) and orthorhombic ZrPt as determined by neutron Rietveld refinement. Electron diffraction indicated that the space group was not body centered, and all refinements were therefore carried out in the space group $P4/m$. Details of the structure will be reported elsewhere. The arc-cast microstructure (Fig. 5) showed a “cored” matrix phase with a small uniform dispersion of light particles. After annealing, we observed small grains ($10\text{--}30\text{ }\mu\text{m}$) of the Zr_9Pt_{11} phase together with a few particles of a second phase.

The neutron diffraction pattern remained essentially unchanged as the sample was heated up to $700\text{ }^{\circ}\text{C}$. At $1000\text{ }^{\circ}\text{C}$

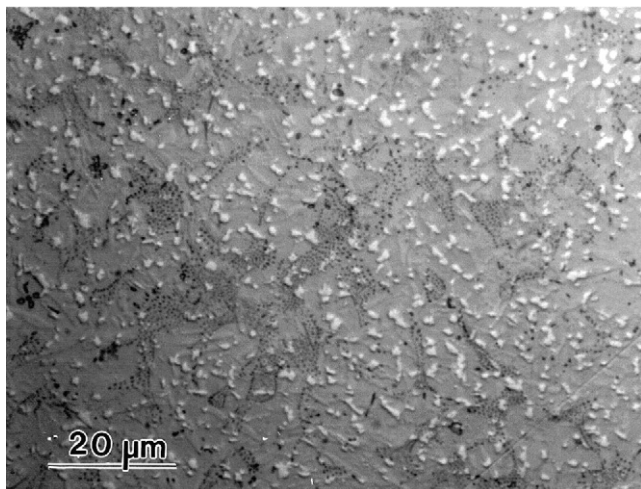


Fig. 5. Photomicrograph of arc-cast Zr_9Pt_{11} .

Rietveld refinement proved conversion of the entire sample to the tetragonal Zr_9Pt_{11} structure, while further heating to $1300\text{ }^{\circ}\text{C}$ produced a mixture of phases. At $1400\text{ }^{\circ}\text{C}$ the tetragonal pattern had been entirely replaced by a rather poorly formed pattern of a rhombohedral Pu_3Pd_4 -type structure (Zr_3Pt_4) along with other phases, perhaps including orthorhombic ZrPt. The rhombohedral pattern persisted to $1600\text{ }^{\circ}\text{C}$. On cooling, peaks of the tetragonal phase reappeared at $1300\text{ }^{\circ}\text{C}$ with a tetragonal/rhombohedral ratio of about 58:42 as determined from the Rietveld refinement. At $1200\text{ }^{\circ}\text{C}$ the ratio was about 63:37 and at $50\text{ }^{\circ}\text{C}$ the sample was still transforming. It continued to transform with time at room temperature so that after 4 weeks we observed a ratio of 70:30. However, the rhombohedral phase had transformed to a presumed triclinic structure such as that found for Zr_3Pt_4 .

The sample was then re-annealed at $1250\text{ }^{\circ}\text{C}$ for 1 h followed by rapid cooling. This produced only a slight change in the phase ratio to about 72:28. The sample was then annealed at $1500\text{ }^{\circ}\text{C}$ for 0.5 h followed by rapid cooling. This produced a complete disappearance of the tetragonal phase, exhibiting only the triclinic Zr_3Pt_4 phase and the emergence of a cubic Cu_3Au -type pattern with $a = 4.051(1)\text{ }\text{\AA}$ at room temperature. This value may be compared with $a = 3.99\text{ }\text{\AA}$ for the Cu_3Au -type compound $ZrPt_4$ [4]. A plot of average atomic volume versus atomic fraction for known Zr–Pt compounds is given in Fig. 6. The lattice constant of $4.051\text{ }\text{\AA}$ implies that this cubic phase has a composition of about $Zr_{30}Pt_{70}$.

In order to confirm the assumption of non-equilibrium conditions in the above experiments, new samples were prepared at the compositions $Zr_{35}Pt_{65}$, Zr_3Pt_4 , Zr_9Pt_{11} and $Zr_{47}Pt_{53}$. These four samples, along with the original Zr_9Pt_{11} sample used for the neutron diffraction experiments, were annealed simultaneously at $1200\text{ }^{\circ}\text{C}$ for 7 days followed by rapid cooling. Nearly identical complex X-ray diffraction patterns were now observed at room temperature for the Zr_3Pt_4 and Zr_9Pt_{11} samples, character-

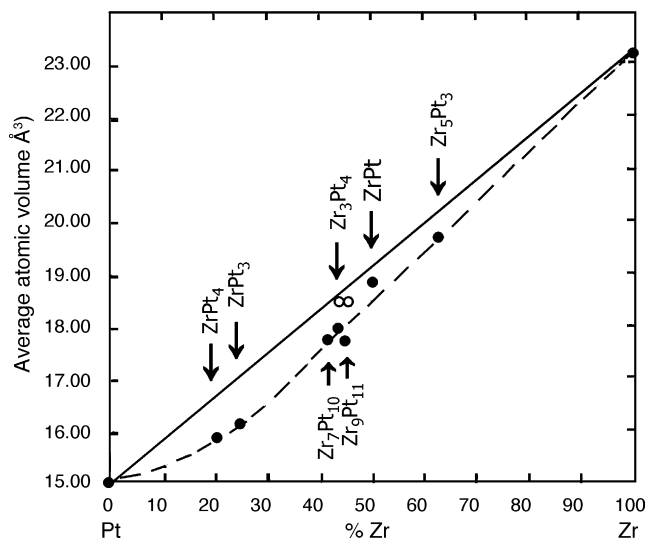


Fig. 6. Average atomic volumes vs. composition for Zr–Pt compounds. For the compounds Zr_3Pt_4 and Zr_9Pt_{11} , the open circles represent the tetragonal phase and the closed circles represent the triclinic/rhombohedral phase.

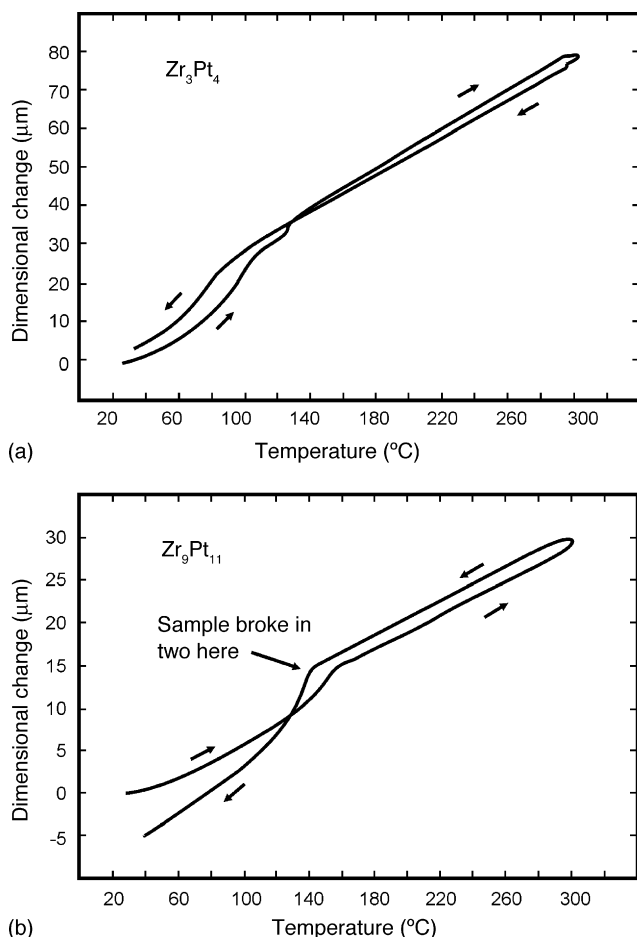


Fig. 7. Thermal expansion curves for (a) Zr_3Pt_4 and (b) Zr_9Pt_{11} , annealed at 1200°C for 7 days.

istic of the triclinic Zr_3Pt_4 -type structure. When these samples were heated, both patterns changed to those of the rhombohedral Zr_3Pt_4 structure over a temperature range centered about 70°C and 140°C , respectively, as determined by neutron diffraction (see below). In both samples the transformation was reversible and occurred over a range of approximately 40° , with coexistence of both triclinic and rhombohedral phases. Measurements of thermal expansion versus temperature (Fig. 7) confirmed these transformation temperatures and led us to conclude that these were diffusionless displacive transformations.

A micrographic examination of these samples revealed surface features (striations and bands) characteristic of displacive transformations. In the case of the Zr_9Pt_{11} sample, we observed a triangular network (Fig. 8) very similar to what was previously reported for Zr_3Rh_4 , in which these triangular networks were associated with the presence of an incommensurate charge density/lattice displacement wave [11]. A small amount of a second phase appears at the grain boundaries in the Zr_9Pt_{11} sample but does not appear in the Zr_3Pt_4 sample. This phase is presumably the same as that identified in subsequent neutron diffraction studies as having a Cu_3Au -type structure with $a \approx 3.98 \text{ \AA}$ at room temperature.

Electron microscopy studies on the Zr_9Pt_{11} sample that was slowly cooled from 1600°C revealed a fine structure (Fig. 9)

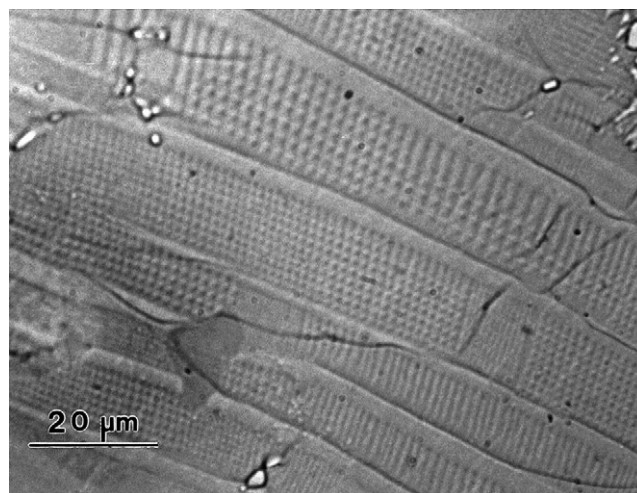


Fig. 8. Photomicrograph of Zr_9Pt_{11} annealed at 1200°C for 7 days, showing triangular domain structure with particles of cubic $ZrPt_4$.

which is not yet understood but will hopefully shed some light on the mechanism of the transformation.

The Zr_9Pt_{11} sample, which had now been annealed at 1200°C for 7 days, was again examined at temperatures from 20 to 1200°C by neutron diffraction. Crystallographic data are given in Table 1. At 20°C only the triclinic phase was present, whereas both the triclinic and rhombohedral phases were present between 100 and 160°C (Table 2). Only the rhombohedral phase was now stable over the entire temperature range of 200 – 1200°C and the tetragonal phase did not reappear. Neutron data were re-collected at 300°C for an accurate determination of the rhombohedral structure parameters. This revealed that the extension of the composition range of the rhombohedral structure for Zr_3Pt_4 (42.9 at.% Zr) to Zr_9Pt_{11} (45 at.% Zr) does not occur by substitution of Zr atoms on Pt sites but rather by the creation of lattice vacancies on these sites. The excess Pt atoms were appar-

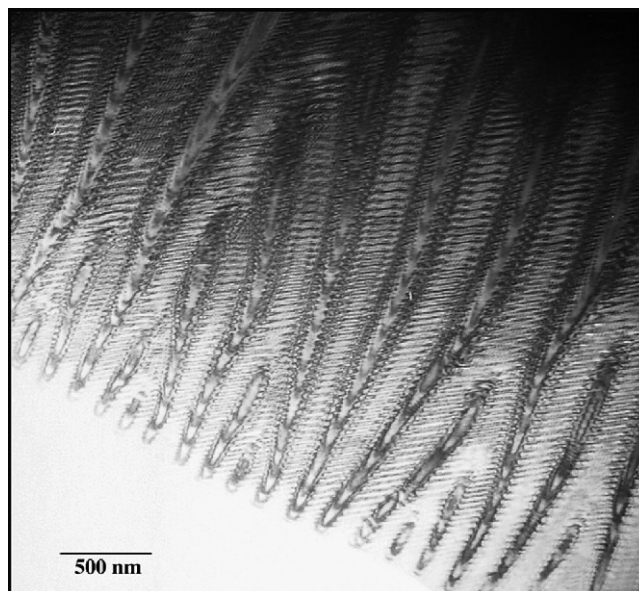


Fig. 9. Electron micrograph of Zr_9Pt_{11} slowly cooled from 1600°C .

Table 2
Phase fractions of triclinic and rhombohedral Zr₉Pt₁₁

Temperature (°C)	Mass fraction triclinic phase (%)	Mass fraction rhombohedral phase (%)
20	94	0
100	86	9
120	77	18
130	68	27
140	55	40
150	13	81
160	5	89
200	0	94

Phase fractions have been calculated using the undoubled triclinic lattice (see text); the fraction of the triclinic phase is likely to be underestimated. The values do not add up to 100% owing to the presence of approximately 5% ZrPt₃. Standard uncertainties are ±5%.

ently removed through the formation of approximately 5 wt.% of a Cu₃Au-type phase ($a = 3.982(1) \text{ \AA}$ at 300 °C) that is presumably Pt-rich.

3.4. Zr₃Pt₄

Phase analysis of the Zr₃Pt₄ material, initially annealed at 1200 °C for 1 h, was complicated by the presence of a previously unreported phase of composition Zr₃Pt₄ which possesses a complex presumably triclinic structure at room temperature. Once the structure of this phase was approximately determined by neutron Rietveld refinement, it was found that the sample as prepared consisted of about 73 wt.% triclinic Zr₃Pt₄ and 23 wt.% tetragonal Zr₉Pt₁₁. This ratio is apparently established by compositional segregation during casting. On heating to 1500 °C during data collection for neutron diffraction analysis, this alloy adopted entirely a rhombohedral Pu₃Pd₄-type structure. The structure remained unchanged on cooling until some tetragonal phase reappeared between 1300 and 1200 °C. Structural refinements using data sets taken at 1200 °C and at every 100 °C interval down to 300 °C all gave a phase composition of 88 wt.% rhombohedral Zr₃Pt₄ and 12 wt.% tetragonal Zr₉Pt₁₁. As in all experiments, the samples were held at temperature until no further changes were observed in the diffraction pattern before data for analysis were collected. Representative crystallographic data are given in Table 1. The sample was allowed to cool slowly to room temperature in the furnace and remained there for about 1 week. In subsequent diffraction experiments, there was no detectable amount of the tetragonal phase in the sample. Evidently, given time, the tetragonal phase transforms to the rhombohedral/triclinic phase after appropriate annealing (in this case, a 2-day neutron diffraction experiment followed by slow cooling). Neutron diffraction studies in the range 50–200 °C confirmed the reversible triclinic to rhombohedral phase transition reported above for the composition Zr₉Pt₁₁. At this composition the transition takes place over the range 50–100 °C, whereas the transition temperature was slightly higher for the Zr₉Pt₁₁ composition. The phase compositions determined by multi-phase Rietveld refinement are given in Table 3.

The Zr₃Pt₄ rhombohedral structure that forms above the relatively low transition temperature is the same as that

Table 3
Phase fractions of triclinic and rhombohedral Zr₃Pt₄

Temperature (°C)	Mass fraction triclinic phase (%)	Mass fraction rhombohedral phase (%)
20	100	0
50	76	24
60	73	27
70	57	43
80	39	61
90	26	74
100	18	82
200	8	92

Phase fractions have been calculated using the undoubled triclinic lattice (see text); the fraction of the triclinic phase is likely to be underestimated. Standard uncertainties are approximately ±5%.

reported for Zr₃Pd₄ [12], rhombohedral Pu₃Pd₄-type, space group $R\bar{3}$, with $Z=6$ for the hexagonal representation. At 100 °C, $a = 12.526(1)$, $c = 5.528(1) \text{ \AA}$ and $V = 751.1 \text{ \AA}^3$ for Zr₃Pt₄; this corresponds to $a = 7.463 \text{ \AA}$, $\alpha = 114.1^\circ$, $Z=2$, $V = 250.5 \text{ \AA}^3$ when referred to the rhombohedral axes. The lower symmetry presumably triclinic modification can most easily be visualized as a triclinic distortion of the rhombohedral representation. At 70 °C, the refined unit cell parameters are $a = 7.517(1)$, $b = 7.404(1)$, $c = 7.484(1) \text{ \AA}$; $\alpha = 112.0(1)$, $\beta = 114.9(1)$, $\gamma = 115.6(1)^\circ$; $V = 250.1 \text{ \AA}^3$. Neutron diffraction data were also collected at 3.5 K in order to better study the structure of the triclinic form. It was found that the actual triclinic lattice is probably doubled in volume according to the transformation matrix $[0 -1 0; -1 0 0; -1 -1 2]$. This results in an “ideal” lattice with $a \approx 7.50$, $b \approx 7.50$, $c \approx 10.4 \text{ \AA}$; $\alpha \approx 99.4$, $\beta \approx 99.4$, $\gamma \approx 114.1^\circ$. At 3.5 K the actual refined lattice parameters are $a = 7.368(1)$, $b = 7.535(1)$, $c = 10.527(1) \text{ \AA}$; $\alpha = 101.7(1)$, $\beta = 97.1(1)$, $\gamma = 116.0(1)^\circ$. Note that this lattice doubling occurs in the direction of the parent c -axis in the hexagonal representation. Although the atomic coordinates were refined for this model assuming space group $P\bar{1}$, single-crystal diffraction work would be necessary in order to confirm the presumed triclinic structure. Fig. 10 shows a portion of the neutron diffraction pattern at 300 °C, where the entire sample is rhombohedral, and at 3.5 K where the sample is triclinic.

3.5. Zr₇Pt₁₀

This sample was arc-cast and annealed at 1200 °C for 1.5 h. The room-temperature neutron diffraction pattern very closely resembled that calculated for the Zr₇Ni₁₀ structure type [13,14]. Crystallographic data are given in Table 1. Structural refinement, however, indicated that the two phases are probably not exactly isostructural. Although there is general agreement between the calculated and observed patterns, the calculation of diffraction intensity where none is observed proves that the model is not quite correct. Calculations modeled after the Zr-rich phase, space group $Pbca$, reported by Kirkpatrick et al. [14] for Zr₇Ni₁₀ resulted in essentially the same agreement as that for the stoichiometric material.

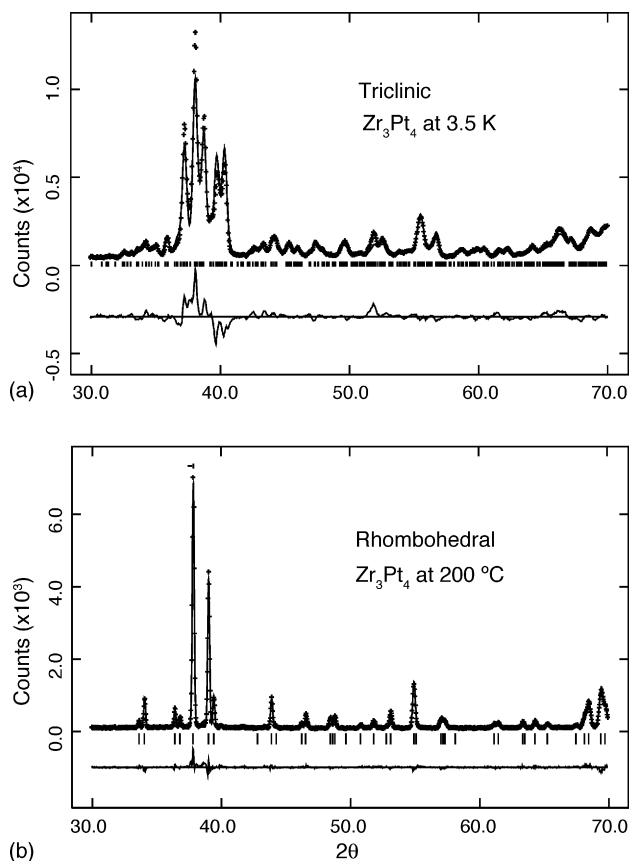


Fig. 10. Observed and calculated intensities for a portion of the neutron diffraction pattern of Zr_3Pt_4 at 200 °C, where the structure is rhombohedral Pu_3Pd_4 -type, and at 3.5 K where the structure distorts to a presumed triclinic symmetry. Data were collected using $\lambda = 1.5403 \text{ \AA}$ at 3.5 K and 2.0775 \AA at 200 °C; for comparison purposes the 200 °C data have been plotted as if collected using $\lambda = 1.54 \text{ \AA}$. At 200 °C the Zr atoms occupy position 18f (x, y, z) with refined parameters $x = 0.0443(3)$, $y = 0.2161(2)$, $z = 0.2256(5)$; the Pt atoms occupy positions 3a (0, 0, 0), 3b (0, 0, 1/2), and 18f with $x = 0.2674(2)$, $y = 0.2148(2)$, and $z = 0.2874(3)$.

4. Discussion

Our studies have shown that the phase equilibria in Pt-rich near-equiatomic Zr–Pt alloys involve mainly B2 derivative structures. The structure of the high-temperature B2 compound, ZrPt, is relatively easy to understand. Each Zr atom lies at the center of a cubic configuration of 8 Pt atoms at a distance of $\sqrt{3}a/2$ (Fig. 11a), where a is the cubic unit cell parameter. The second shell around this central Zr atom consists of an octahedral configuration of 6 Zr atoms at a distance of a . This simple structure can be regarded as arising from strong localized bonds between the Zr and Pt atoms and much weaker interactions between two Zr atoms or two Pt atoms.

Substitution of a Pt atom for the central Zr atom (resulting in an anti-site Pt atom) will have a profound effect on structural stability. Strong Zr–Pt bonds to the cube sites will be replaced by much weaker Pt–Pt bonds and the formerly weak Zr–Zr bonds to the octahedral sites will be replaced by strong Zr–Pt bonds. The octahedral configuration will experience a strong inward force while the cubic configuration will tend to be displaced outward. One can see displacements of this type around the anti-

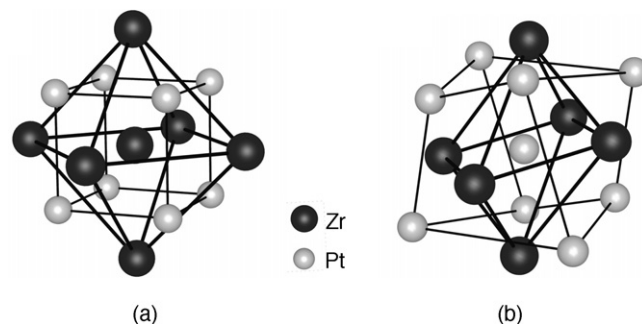


Fig. 11. Nearest neighbors of (a) Zr in B2-type ZrPt and (b) anti-site Pt in rhombohedral Zr_3Pt_4 . The central Pt atom in the Zr_3Pt_4 structure now has Zr atoms as nearest neighbors and the shorter Zr–Pt bonds result in distortion of the parent B2-type structure.

site Pt atoms in the B2 derivative structure of the Pu_3Pd_4 -type compound Zr_3Pt_4 (Fig. 11b) [15]. These displacements result in the more complex structures and phase equilibria found here for the Zr–Pt system.

A fully ordered B2 ZrPt structure is composed of superimposed square atomic networks that consist alternately of all Pt atoms and all Zr atoms. This structure can, therefore, accommodate excess Pt atoms simply by substituting them for some of the atoms in the “all Zr” networks. The disruptive influence of such substitutions can be minimized by incorporating them in an ordered manner. It has been shown [16] that this will produce binary structures whose compositions are defined by the formula ratio $n - 1/n + 1$ where n is any integer. The structure of the compounds Zr_3Pt_4 and Zr_9Pt_{11} are examples of such B2 derivative structures in which $n = 7$ and $n = 10$, respectively.

Anti-site atoms are, of course, not the only source of instabilities in B2 structures. The fully ordered equiatomic ZrPt compound is only stable at high temperatures, and transforms from a B2-type structure to a CrB-type structure by a diffusionless martensitic reaction at 1590 °C. This phase transformation has its counterpart in the compound ZrPd except that the latter occurs at the much lower temperature of 620 °C [17]. A “shuffle” mechanism for this transformation has been previously proposed [18]. It is uncertain whether the B2 phase region extends to Pt-rich compositions or whether a two-phase region separates it from the structure that was observed above 1550 °C in the alloy $Zr_{47}Pt_{53}$. We have chosen to regard it as a continuous single-phase region in our phase diagram. In either case, the high temperature phase of the alloy $Zr_{47}Pt_{53}$ is probably the source of the Widmanstätten structures in Figs. 2 and 4. Our neutron diffraction high temperature measurements indicate that the high-temperature $Zr_{47}Pt_{53}$ phase equilibrates with a rhombohedral phase above 1550 °C and that the rhombohedral phase equilibrates with orthorhombic ZrPt at lower temperatures.

Our solidus measurement at $1920 \pm 10 \text{ °C}$ in the Zr_9Pt_{11} alloy is believed to indicate a peritectic reaction between the B2-related $Zr_{47}Pt_{53}$ phase and the liquid phase that produces the rhombohedral phase at the composition Zr_9Pt_{11} (55% Pt). The photomicrograph of the partially melted alloy (Fig. 12) shows a typical peritectic ring structure and in some areas we see a double ring structure indicative of a second peritectic reaction. We also

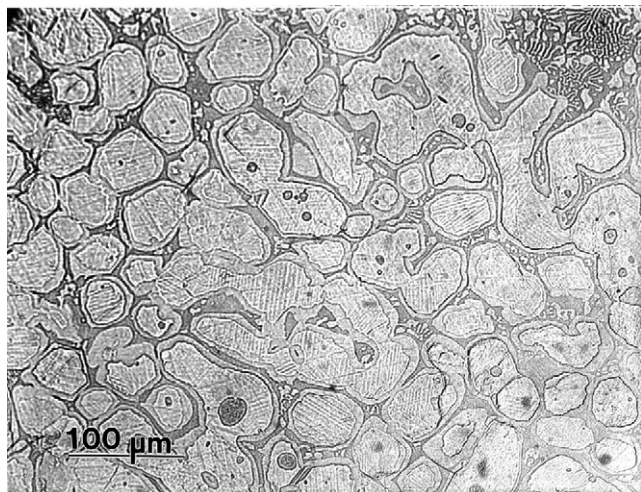


Fig. 12. Photomicrograph of partially melted Zr_9Pt_{11} , exhibiting primary particles of martensitic $ZrPt$ with peritectic rings of Zr_3Pt_4 and small regions of eutectic ($Zr_7Pt_{10} + ZrPt_3$).

see some eutectic structure. This eutectic structure comprises nearly 100% of the alloy $Zr_{35}Pt_{65}$ and has a solidus temperature of 1720°C . The solidus temperature of the alloy Zr_7Pt_{10} was slightly higher at 1740°C .

We had considerable difficulty establishing the phase equilibria in alloys containing the compounds Zr_3Pt_4 and Zr_9Pt_{11} . Successive diffraction experiments at different temperatures produced time-dependent behavior which sometimes seemed inconclusive, inconsistent and even contradictory. To clarify this behavior we prepared new samples that we annealed simultaneously at 1200°C for 7 days. We found that the alloy Zr_9Pt_{11} , which has the tetragonal structure when annealed at 1200°C for 1 h, instead when annealed at 1200°C for 7 days has a structure that is triclinic at room temperature and rhombohedral Pu_3Pd_4 -type at higher temperatures. (This triclinic/rhombohedral structure is hereafter referred to as the rhombohedral phase.) The rhombohedral phase was found to be stable over a small composition range from its ideal Zr_3Pt_4 (42.9% Zr) to Zr_9Pt_{11} (45.0% Zr). Since Zr_3Pt_4 is a fully ordered structure, we expected that Zr atoms must substitute for some of the Pt atoms in Zr_3Pt_4 in order to produce a more Zr-rich composition. However, Rietveld refinement of atomic occupancies for the Zr-rich composition at 300°C shows conclusively that the rhombohedral structure instead obtains the Zr-rich composition by creating vacancies on lattice sites occupied by Pt atoms, specifically those at (000) and (00 1/2). We found that the excess Pt atoms are retained in the alloy as part of a metastable phase having a cubic Cu_3Au -type structure with $a = 3.985 \text{ \AA}$ at 300°C . This is close to the value reported for the Cu_3Au -type compound $ZrPt_4$ ($a = 3.99 \text{ \AA}$).

When we examined the alloy $Zr_{47}Pt_{53}$, also annealed at 1200°C for 7 days, we expected to find a two-phase structure consisting of the phase $ZrPt$ with the rhombohedral vacancy-stabilized Zr_9Pt_{11} phase. Instead, we observed the phase $ZrPt$ along with the tetragonal Zr_9Pt_{11} phase. At or around the composition $Zr_{45}Pt_{55}$ (Zr_9Pt_{11}) there is apparently a delicate competition for stability between the vacancy-containing rhombohedral structure and the vacancy-free tetragonal structure. Small con-

tributions to the free energy of either phase that are ordinarily inconsequential can in this instance be the “feather that turns the scale”. The critical feature here is whether the phase Zr_3Pt_4 is supersaturated with Pt or with Zr. If with Pt, then precipitation of $ZrPt_4$ can occur and the vacancy-stabilized rhombohedral Zr_9Pt_{11} compound will form. If with Zr, then precipitation of $ZrPt_4$ cannot occur and the vacancy-free tetragonal compound will form. [The composition difference between the vacancy-stabilized rhombohedral phase and the tetragonal phase is apparently quite small and it seems unlikely that a two-phase region would separate them. A second-order transition might occur, however, by simply rearranging the anti-site atoms in these two structures. This remains to be verified if it indeed occurs.]

The tetragonal phase is not stable above 1300°C but vacancy formation in the rhombohedral phase can apparently still occur by precipitation of the Pt-rich Cu_3Au -type phase, which in this case may have a composition of about $Zr_{30}Pt_{70}$ based on its observed lattice parameter ($a = 4.051 \text{ \AA}$ at room temperature). Its formation involves a diffusion process, however, and it will proceed only as far as time permits. Areas of the sample that remain unaffected by this diffusion will again transform to the tetragonal structure on cooling below 1400°C . This will result in a mixture of retained rhombohedral phase and newly created tetragonal phase.

The formation of the triclinic phase on cooling from a prior rhombohedral phase involves a displacive transformation that has both athermal and isothermal characteristics. It is a completely reversible transformation and is never associated with the tetragonal structure.

By combining the information given by Kendall et al. [3] and Fairbank et al. [4] with the results of the present study we have constructed a complete phase diagram for the Zr–Pt system (Fig. 13). The previous studies lacked solidus data for Pt-rich

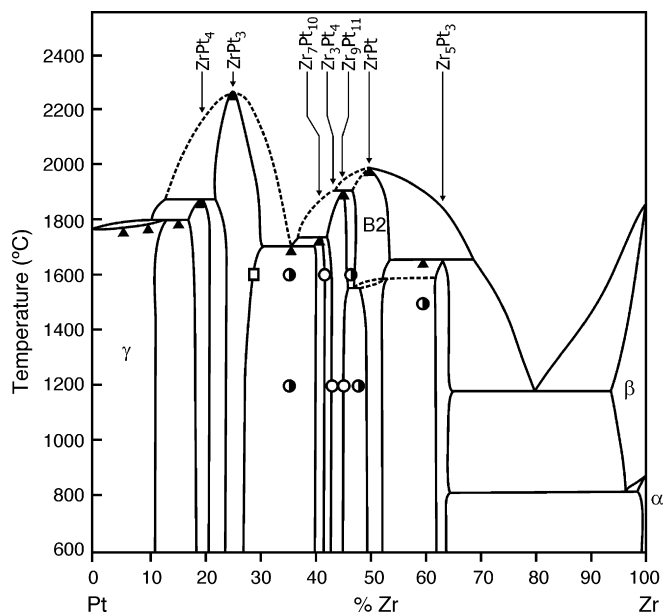


Fig. 13. Phase diagram of the Zr–Pt system. The triangles indicate the onset of melting on heating; the square indicates that the composition was determined by EDS; half-filled circles indicate a two-phase alloy; the open circles indicate a single-phase alloy.

alloys, which we have obtained in the present study. We observed the peritectic transformation of $ZrPt_4$ at $1880 \pm 10^\circ C$ and the congruent melting of $ZrPt_3$ at $2250^\circ C$.

High-temperature neutron diffraction experiments have proven to be a rich source of information about these alloys. For example, the existence of the compound Zr_3Pt_4 and the complex associated phase equilibria would have been difficult to probe by other techniques. We expect that further work may be required to understand fully the Zr–Pt system.

Acknowledgements

We wish to thank Ms. Sandy Claggett for her extraordinary patience and persistence in preparing our very brittle and heat-sensitive samples for electron microscopy, and Dr. Leo Bendersky for performing the measurements. Ms. Maureen Williams obtained numerous X-ray diffraction patterns for us and Dr. Alex Shapiro contributed helpful information on certain phase compositions using EDS analysis. Mr. Tony Giuseppetti conducted the thermal expansion experiments. We also thank Dr. Robert Shull for generously providing high-purity platinum.

References

- [1] P.J. Meschter, W.L. Worrell, *Metall. Trans. A* 8 (1977) 503.
- [2] L. Topor, O.J. Kleppa, *J. Less-Common Met.* 155 (1989) 61.
- [3] E.G. Kendall, C. Hays, R.E. Swift, *Trans. Metall. Soc. AIME* 22 (1961) 445.
- [4] G.B. Fairbank, C.J. Humphreys, A. Kelly, C.N. Jones, *Intermetallics* 8 (2000) 1091.
- [5] A. Raman, K. Schubert, *Z. Metallk.* 55 (1964) 704.
- [6] A.E. Dwight, R.A. Conner, J.W. Downey, *Acta Crystallogr.* 18 (1965) 835.
- [7] S.C. Panda, S. Bahn, *J. Less-Common Met.* 34 (1965) 344.
- [8] A.C. Larson, R.B. Von Dreele, *General Structure Analysis System (GSAS)*, Los Alamos National Laboratory Report No. LAUR-86-748, 2004.
- [9] P. Wodniecki, B. Wodniecka, A. Kulinska, M. Uhrmacher, K.P. Lieb, *J. Alloys Compd.* 399 (2005) 52.
- [10] L.A. Bendersky, J.K. Stalick, R. Portier, R.M. Waterstrat, *J. Alloys Compd.* 236 (1996) 19.
- [11] L.A. Bendersky, R.M. Waterstrat, *J. Alloys Compd.* 252 (1997) L5.
- [12] L.A. Bendersky, J.K. Stalick, R.M. Waterstrat, *J. Alloys Compd.* 201 (1993) 121.
- [13] J.M. Joubert, R. Cerny, K. Yvon, M. Latroche, A. PercheronGuegan, *Acta Crystallogr. C* 53 (1997) 1536.
- [14] M.E. Kirkpatrick, J.F. Smith, W.L. Larson, *Acta Crystallogr.* 15 (1962) 894.
- [15] L.H. Bennett, R.M. Waterstrat, L.J. Swartzendruber, L.A. Bendersky, H.J. Brown, R.E. Watson, *J. Appl. Phys.* 87 (2000) 6016.
- [16] K. Cenzual, J.L. Jorda, E. Parthé, *Acta Crystallogr. C* 44 (1988) 14.
- [17] R.M. Waterstrat, A. Shapiro, A. Jeremie, *J. Alloys Compd.* 290 (1999) 63.
- [18] R.M. Waterstrat, L.A. Bendersky, R. Kuentzler, *Mater. Res. Soc., Symp. Proc.* 246 (1992) 115.